


ORIGINAL RESEARCH

Open Access



Seismic site characterization at the western Cephalonia Island in the aftermath of the 2014 earthquake series

I. Kassaras* , P. Papadimitriou, V. Kapetanidis and N. Voulgaris

*Correspondence:
kassaras@geol.uoa.gr
Department
of Geophysics-Geothermics,
Faculty of Geology
and Geoenvironment,
National Kapodistrian
University of Athens,
Panepistimiopolis,
15784 Zografou, Athens,
Greece

Abstract

Background: The site response during a strong earthquake event may be proven crucial for earthquake hazard assessment and risk mitigation. Two moderate magnitude earthquakes that occurred in early 2014 in Cephalonia produced the largest ground motion values ever recorded in Greece, highly exceeding the provisions of the effective seismic code implying for local effects. This motivated the investigation of site response in the epicentral area presented herein.

Methods: We applied the HVSR method on free-field ambient noise measurements obtained during an in situ survey. 68 measurements were adopted for site characterization after their validation using earthquakes and geotechnical data. The site response was approximated by the peak frequency and the amplification ratio of the HVSR curves.

Results: The majority of measurements exhibit smooth lateral variations in the frequency range 0.7–17 Hz, at a factor up to 7 and they are clearly classified in two bands, a low (0.7–4 Hz) and a high one (5–17 Hz). Some discrepancies that are observed between microtremor measurements and earthquake recordings for peak frequencies <2 Hz and overall underestimated ambient noise HVSR amplification are likely explained by near-source, radiation pattern and/or nonlinear soil effects.

Conclusions: High frequencies combined with low amplification correlate with damage in the hardest hit areas. Low frequencies are aligned in a NNE-SSW direction in the epicentral area, similar to the strike of the activated fault, indicating that the properties of rocks along the fault zone have possibly been affected by slippage and/or dynamic effects.

Keywords: Site effects, Microtremors, HVSR, Cephalonia

Background

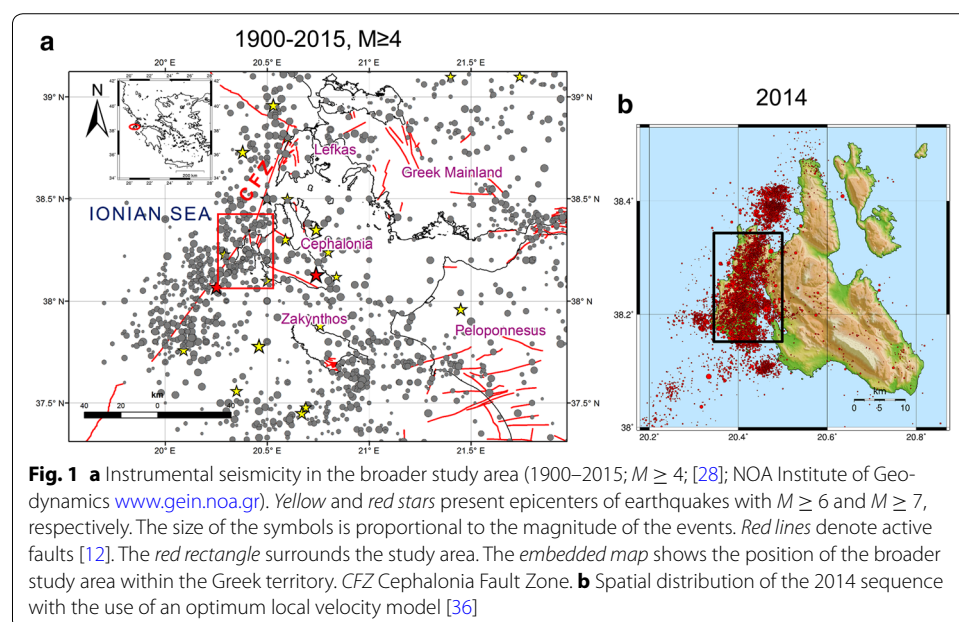
Site effects play a critical role in the configuration of the seismic motion at a location and hence they are considered in principle in seismic standards. However, it has been globally manifested for numerous cases of devastating earthquakes that the generic provisions provided by effective seismic codes are grossly misleading, with the observed strong ground motion parameters and coseismic effects being far higher than predicted [50]. Surprisingly, this was the case during the recent earthquake doublet that occurred

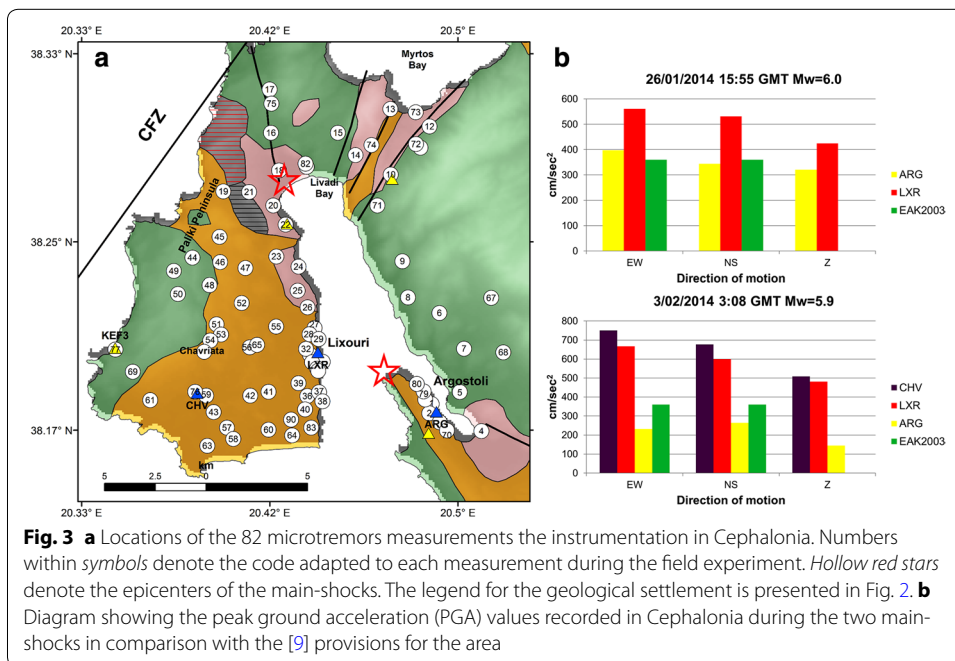
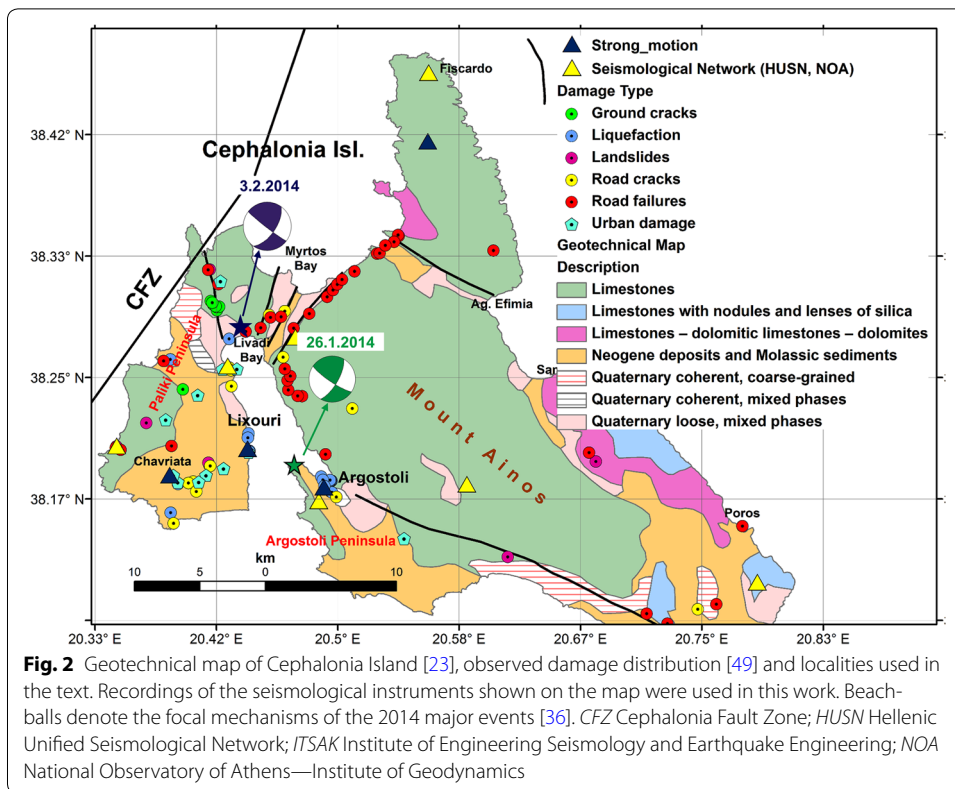
in western Cephalonia on 26.1.2014 with $M_w = 6.0$ and on 3.2.2014 with $M_w = 5.9$ [37] regarding (a) an extremely high PGA and spectral acceleration recorded near the epicentral area largely exceeding the provisions of the National Seismic Code [9] and (b) rather irregular co-seismic effects distribution at both the urban and rural environment. Near-fault effects and site conditions [46] are suggested to have played a significant role. In this work we present the detailed investigation of site response in the epicentral area of the 2014 earthquake sequence.

The study area is the western part of Cephalonia Island (Fig. 1). Cephalonia is dominated by the NNE-SSW striking Cephalonia Fault Zone (CFZ in Fig. 1). CFZ is considered to be the most hazardous tectonic feature in the region, proven capable to produce earthquakes with $M > 7$. The geology in Cephalonia consists of an Alpine basement including the Ionian and Paxos thrust and fold units [4] and two main series of post-Alpine formations that are deposited over the Alpine basement [23].

Cephalonia belongs to the highest zone (III) of the current Greek seismic code [9] as one of the most seismically prone areas in Europe [45]. During the historical period (<1900) 13 earthquakes with (estimated) $M \geq 6.0$ have been reported in the region. The strongest event with $M_{7.4}$ occurred on 4.2.1867 [38]. Since 1900, 11 earthquakes with $M_s \geq 6.0$ occurred in the region [28]. Five of them took place in 1953 with the largest event having $M_{7.3}$. The latest strong event with $M_{6.7}$ took place on 17.1.1983 approximately 30 km SW of Lixouri.

On 26.1.2014 and 3.2.2014 two moderate earthquakes with $M_w = 6.0$ and $M_w = 5.9$, respectively, occurred onshore at the western part of Cephalonia having ruptured two 10+ km long strike-slip faults (Fig. 2; [13, 20]) fortunately without causing any casualties but only structural damage [37] and environmental effects [49]. GPS results revealed large amplitudes of displacement in both horizontal (6–40 cm) and vertical (8–15 cm) components in the vicinity of Paliki peninsula, primarily attributed to these earthquakes [13, 42]. Maximum macroseismic intensities $I_{max} = VII$ were observed during the event





on 26.1.2014 and $I_{max} = VIII+$ during the event on 3.2.2014 at the southern part of Paliki peninsula [37]. Figure 2 presents the co-seismic damage due to the two main-shocks concentrated mostly in Paliki peninsula [49].

Ground motion during the main-shocks on 26.1.2014 ($M_w = 6.0$) and 3.2.2014 ($M_w = 5.9$) was recorded by three accelerographs located in the epicentral area (ARG, LXR, CHV) (Fig. 3a). The recordings in Paliki peninsula (LXR, CHV) indicated high acceleration (Fig. 3b). The CHV temporary accelerograph installed by ITSAK (Fig. 3a) recorded peak ground acceleration (PGA) of ~ 0.75 g for the latter event, highly exceeding the Greek Seismic Code provisions (0.36 g for a return period of 475 years; [9]) being the highest ever recorded in Greece (Fig. 3b). Both LXR and CHV stations fall in the near-fault area at an epicentral distance ~ 10 km [46].

This sequence includes numerous events with $M_w > 4$, occupying an area having a length of about 30 km beneath Paliki Peninsula, about 10 km eastern than the forecasted CFZ zone (Fig. 1b). This arrangement suggests that hazard lies closer to the urban environment than expected, as proposed by Hatzfeld et al. [18] and therefore the effective seismic zonation and seismic hazard provisions in the area should be revised. Toward this scope, we introduce experimental site-specific amplification functions for the first time in the area to be utilized in future small-scale earthquake hazard models. The data analyzed are ambient noise, weak and strong motion earthquake recordings and geotechnical observations. The soil response is assessed at 68 positions in the epicentral area located within and near urban areas and its correlation with local geology, active tectonics and post-seismic observations is presented and discussed herein.

Methods

Local site effects were approximated by applying the popular Nakamura technique [32, 33] which is based on the horizontal to vertical spectral ratio (HVSr) of ambient noise recordings at a site, using a three-component seismograph. The method is based on the assumption that the vertical ground motion is not amplified by the surficial layers and hence the ratio of the horizontal over the vertical component corresponds to the transfer function between the seismic basement and the surface. The method consists of recording several minutes of ambient noise vibrations and calculating the ratio of the horizontal to vertical component's Fourier amplitude spectra. The HVSr technique is simple, fast and cost effective, having been widely used in microzonation studies yielding worthy and consistent site characterization models. Numerous theoretical and experimental studies, conducted on the consistency of the method, confirmed the relevance between the fundamental frequency of ambient noise HVSr and the response of the superficial soil (e.g. [2, 30, 35, 44]).

It is widely accepted that the frequency of the HVSr peak correlates well with the fundamental frequency of the surficial layers (e.g. [29, 30, 44]). The HVSr ratio, since it is sensitive to a variety of parameters [3] has been found at times to underestimate the actual site amplification [2, 15, 44]. However, several experimental studies reveal a satisfactory correlation between the HVSr and the site amplification (e.g. [40]). In Greece, the HVSr technique has been frequently applied, providing consistent results with geotechnical borehole data and geophysical measurements (e.g. [1, 6, 21, 24, 26, 27, 34, 43, 47]).

Data

The data used in this study include ambient noise recordings, geotechnical information and earthquake recordings:

Ambient noise measurements

In May 2014 our research team conducted a field survey in western Cephalonia and measured microtremors at 82 selected points, aiming to cover not only the most damaged sites, but also the activated area and to sample the urban centers as much as possible (Fig. 3a). The instruments used were 3-channel Reftek-72A 24-bits digitizers equipped with Güralp CMG40T three-component sensors having natural frequencies 1 and 0.033 Hz, respectively. The exact location of the measurements points was decided in situ by their accessibility and the absence of artificial sources, especially near the residential areas. The measurements were carried out at day time, working hours. To protect from the windy weather conditions, the sensors were buried and sheltered. The sampling frequency was set to 125 sps, the pre-amplification gain was set to 1 and the duration of each record was 20–25 min long. The geographical coordinates of the measurements positions were determined using handheld GPS devices with an uncertainty of ± 10 m. All the equipment was transported by cars which served as the recording centers.

Geotechnical data

Geotechnical data were provided by the Geotechnical Division of the Ministry of Environment, Energy and Climate Change [51] and concern 34 shallow boreholes at depths between 2.5 and 25 m along the road network in Paliki peninsula. These boreholes were conducted prior to the roads maintenance and reconstruction after serious damage due to the 2014 main-shocks.

Earthquake recordings

The data analyzed are (a) acceleration recordings of the main-shocks on 26.1.2014 and 3.2.2014, recorded at three accelerometric stations and (b) their aftershocks recorded by a local seismological network composed of four broadband stations that were installed by the National Observatory of Athens in the epicentral area (Figs. 2, 3a).

Results

Microtremor measurements and their analysis

The ambient noise time series were corrected for baseline mean and trend and were tapered with a 5% cosine function at both ends. Instrumental response correction was performed by considering the poles and zeroes configurations suggested by the manufacturer of the sensors and sensitivity values per component, according to each instrument's calibration sheet. HVSR curves were computed using the GEOPSY software [44] which allows the implementation of several processing tools (filtering, smoothing, windowing, etc.) and quick visualization of the results through a user friendly interface. The analysis was performed in the frequency range of engineering interest 0.5–20 Hz. The Fast Fourier Transform (FFT) was calculated for each component of the data and the spectra were smoothed using a (Konno and Ohmachi [22]) logarithmic window with a smoothing factor of the order of 15–20. The procedure was applied to 5% overlapping variant length windows of stationary signal after removing transients through STA/LTA anti-triggering. HVSR was calculated for each temporal window by the ratio between the smoothed geometric mean of the horizontal components over the vertical one. At

each site the final HVSR curve results from the logarithmic averaging of HVSR curves for each temporal window and its standard deviation.

The analysis of the microtremor time series yielded 82 HVSR curves. As expected, their majority exhibited clear peaks, implying for strong impedance between the superficial loose deposits and the underlain bedrock. The shapes of the HVSR curves are not uniform. Most of them have one peak which sometimes broadens or splits in two peaks at a higher frequency. A few measurements presented almost flat HVSR curves,

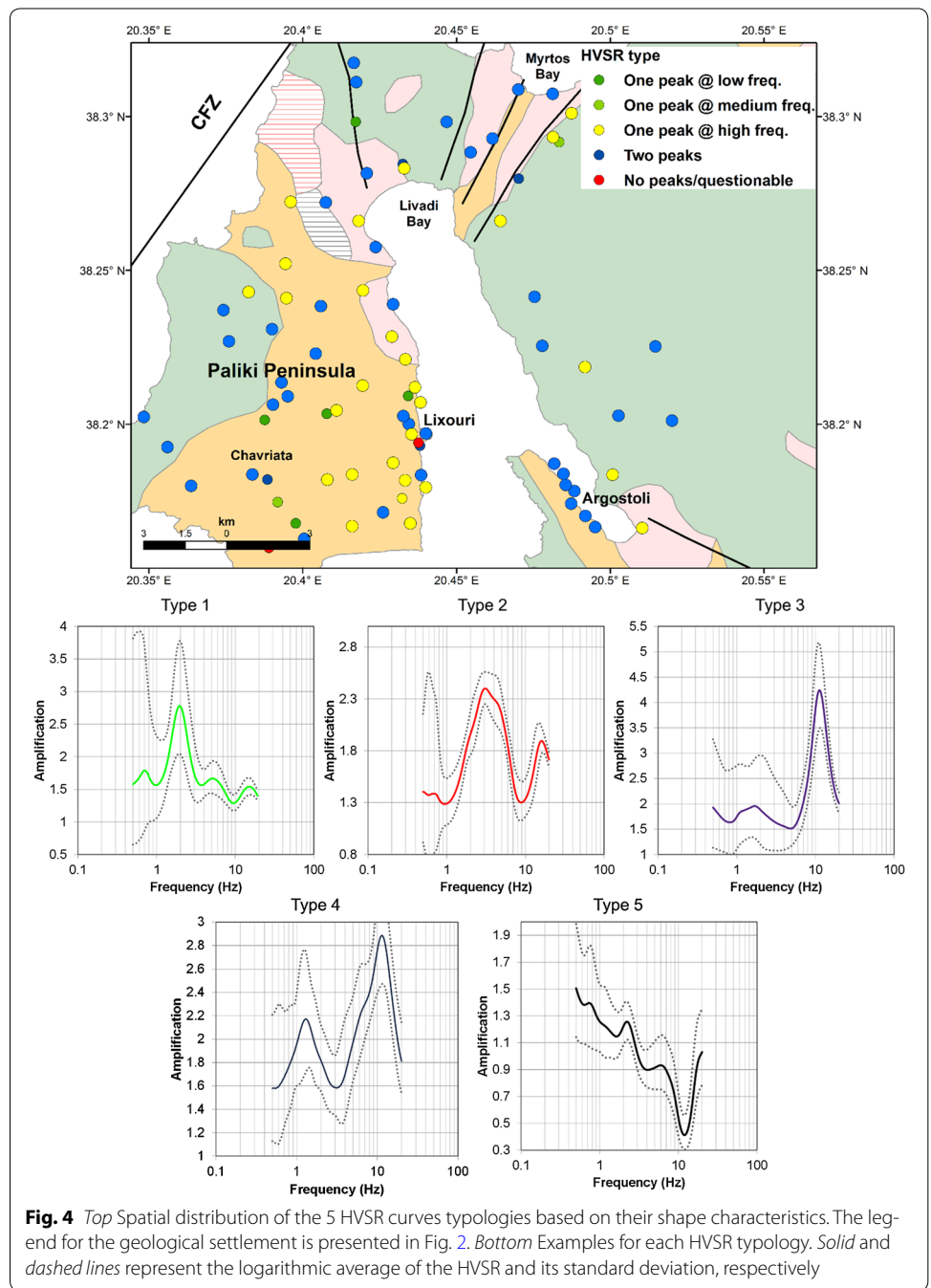


Fig. 4 Top Spatial distribution of the 5 HVSR curves typologies based on their shape characteristics. The legend for the geological settlement is presented in Fig. 2. Bottom Examples for each HVSR typology. Solid and dashed lines represent the logarithmic average of the HVSR and its standard deviation, respectively

Table 1 Summary of the results presenting the primary, F_0 and secondary (where observed), F_1 , peak frequencies and their corresponding amplification factors A_0 and A_1 at 68 measurement sites (Fig. 3a)

| Code | Lat (°) | Lon (°) | F_0 (Hz) | A_0 | F_1 (Hz) | A_1 | Code | Lat (°) | Lon (°) | F_0 (Hz) | A_0 | F_1 (Hz) | A_1 |
|------|---------|---------|------------|-------|------------|-------|------|---------|---------|------------|-------|------------|-------|
| 1 | 38.1783 | 20.4883 | 1.98 | 2.78 | | | 42 | 38.1820 | 20.4080 | 9.50 | 2.49 | | |
| 2 | 38.1742 | 20.4873 | 2.57 | 1.64 | | | 44 | 38.2430 | 20.3824 | 7.87 | 2.31 | | |
| 3 | 38.1702 | 20.4919 | 1.98 | 2.38 | | | 45 | 38.2522 | 20.3944 | 7.87 | 6.00 | 1.91 | 4.89 |
| 4 | 38.1663 | 20.5104 | 6.60 | 1.86 | | | 46 | 38.2410 | 20.3947 | 5.84 | 2.88 | | |
| 5 | 38.1836 | 20.5008 | 11.50 | 4.23 | | | 47 | 38.2384 | 20.4059 | 0.85 | 3.44 | | |
| 6 | 38.2186 | 20.4918 | 5.42 | 2.46 | | | 48 | 38.2309 | 20.3900 | 0.95 | 3.33 | | |
| 7 | 38.2028 | 20.5027 | 2.86 | 5.80 | 14.87 | 5.4 | 49 | 38.2371 | 20.3742 | 3.34 | 2.72 | | |
| 8 | 38.2255 | 20.4779 | 3.88 | 1.30 | | | 50 | 38.2270 | 20.3760 | 1.31 | 5.15 | 12.94 | 3.55 |
| 9 | 38.2414 | 20.4754 | 3.45 | 2.33 | 14.40 | 2.7 | 51 | 38.2136 | 20.3931 | 0.67 | 2.24 | 2.80 | 1.80 |
| 12 | 38.3011 | 20.4874 | 11.43 | 2.60 | 2.21 | 1.75 | 52 | 38.2230 | 20.4042 | 0.67 | 3.37 | 2.48 | 2.50 |
| 13 | 38.3088 | 20.4701 | 1.09 | 2.23 | | | 53 | 38.2091 | 20.3951 | 1.08 | 4.37 | | |
| 14 | 38.2884 | 20.4546 | 2.13 | 3.40 | | | 54 | 38.2064 | 20.3903 | 3.00 | 2.02 | | |
| 15 | 38.2983 | 20.4468 | 1.84 | 2.05 | | | 55 | 38.2126 | 20.4195 | 5.00 | 4.20 | 0.84 | 4.02 |
| 17 | 38.3175 | 20.4166 | 2.27 | 2.52 | | | 58 | 38.1628 | 20.4005 | 3.88 | 1.65 | | |
| 18 | 38.2816 | 20.4208 | 1.41 | 3.47 | 5.43 | 2.8 | 60 | 38.1669 | 20.4161 | 11.87 | 1.93 | | |
| 19 | 38.2723 | 20.3961 | 5.84 | 6.90 | 0.98 | 5.13 | 61 | 38.1800 | 20.3637 | 1.27 | 2.95 | 10.23 | 1.90 |
| 20 | 38.2661 | 20.4182 | 6.01 | 2.23 | | | 65 | 38.2045 | 20.4110 | 13.27 | 5.61 | | |
| 21 | 38.2721 | 20.4075 | 3.22 | 3.18 | | | 67 | 38.2253 | 20.5147 | 4.00 | 1.11 | | |
| 22 | 38.2576 | 20.4237 | 3.34 | 2.98 | | | 68 | 38.2012 | 20.5201 | 3.10 | 0.75 | | |
| 23 | 38.2435 | 20.4196 | 11.01 | 3.10 | 1.59 | 2.20 | 69 | 38.1926 | 20.3560 | 1.42 | 2.82 | | |
| 24 | 38.2390 | 20.4294 | 2.06 | 2.00 | | | 70 | 38.1666 | 20.4951 | 1.47 | 2.14 | | |
| 25 | 38.2285 | 20.4290 | 4.02 | 2.15 | | | 71 | 38.2661 | 20.4643 | 7.18 | 2.26 | | |
| 26 | 38.2211 | 20.4334 | 6.70 | 1.82 | | | 72 | 38.2933 | 20.4814 | 11.87 | 2.50 | 2.57 | 1.82 |
| 27 | 38.2120 | 20.4365 | 6.01 | 2.15 | | | 73 | 38.3074 | 20.4813 | 1.27 | 2.17 | 11.01 | 2.90 |
| 29 | 38.2071 | 20.4383 | 6.45 | 1.95 | | | 74 | 38.2929 | 20.4617 | 1.77 | 1.94 | | |

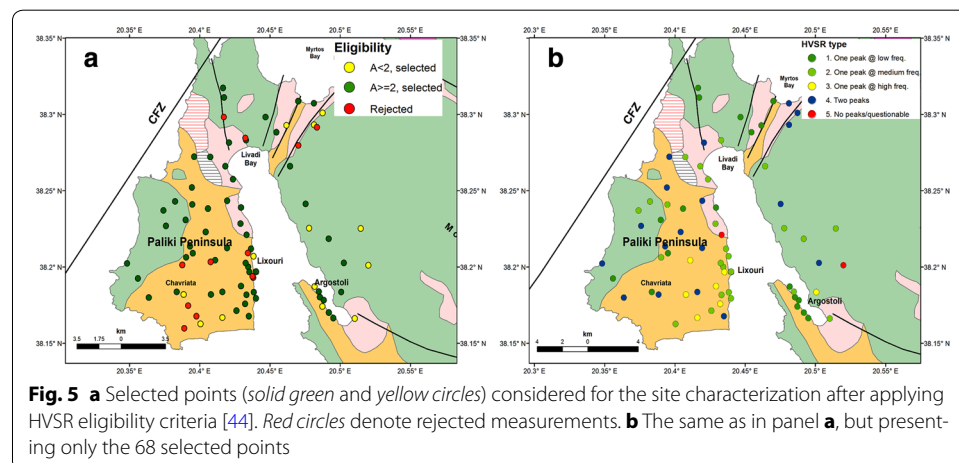
Table 1 continued

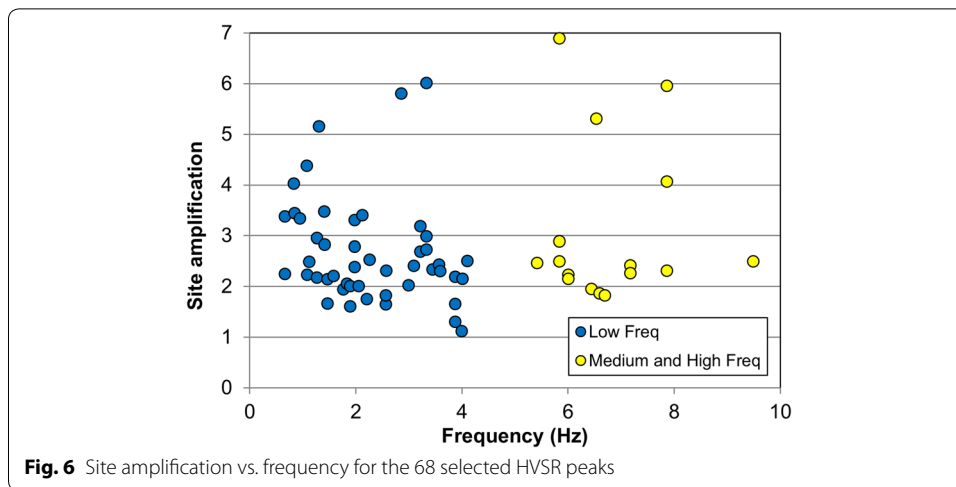
| Code | Lat (°) | Lon (°) | F ₀ (Hz) | A ₀ | F ₁ (Hz) | A ₁ | Code | Lat (°) | Lon (°) | F ₀ (Hz) | A ₀ | F ₁ (Hz) | A ₁ |
|------|---------|---------|---------------------|----------------|---------------------|----------------|------|---------|---------|---------------------|----------------|---------------------|----------------|
| 30 | 38.2001 | 20.4345 | 3.10 | 2.40 | 3.10 | 2.40 | 75 | 38.3112 | 20.4174 | 1.98 | 3.30 | 1.98 | 3.30 |
| 31 | 38.197 | 20.4401 | 3.34 | 6.01 | 3.34 | 6.01 | 76 | 38.1837 | 20.3836 | 1.90 | 2.00 | 1.90 | 2.00 |
| 32 | 38.2027 | 20.4327 | 3.22 | 2.68 | 3.22 | 2.68 | 77 | 38.2024 | 20.3483 | 3.74 | 2.90 | 3.74 | 2.90 |
| 33 | 38.1968 | 20.4354 | 12.32 | 2.90 | 12.32 | 2.90 | 78 | 38.1803 | 20.4855 | 2.58 | 2.31 | 2.58 | 2.31 |
| 36 | 38.1818 | 20.4333 | 7.18 | 2.41 | 7.18 | 2.41 | 79 | 38.1839 | 20.4848 | 3.60 | 2.30 | 3.60 | 2.30 |
| 37 | 38.1835 | 20.4385 | 3.57 | 2.43 | 3.57 | 2.43 | 80 | 38.1872 | 20.4818 | 1.47 | 1.66 | 1.47 | 1.66 |
| 38 | 38.1795 | 20.4400 | 7.87 | 4.06 | 7.87 | 4.06 | 81 | 38.2832 | 20.4330 | 6.54 | 5.30 | 6.54 | 5.30 |
| 39 | 38.1875 | 20.4294 | 16.60 | 5.48 | 16.60 | 5.48 | 83 | 38.1678 | 20.4350 | 5.84 | 2.51 | 5.84 | 2.51 |
| 41 | 38.1837 | 20.4161 | 4.11 | 2.50 | 4.11 | 2.50 | 90 | 38.1714 | 20.4261 | 3.88 | 2.19 | 3.88 | 2.19 |

suggesting no site amplification. Figure 4 presents the spatial distribution of the HVSR curves divided into five typologies according to their shape: (1) having one peak at low frequencies in the range 0–4 Hz, (2) having one peak at medium frequencies in the range 5–9 Hz, (3) having one peak at high frequencies in the range 10–17 Hz, (4) having two peaks and (5) having questionable or no peaks.

We applied eligibility criteria introduced by the SESAME project [44] related to the shape and the peak frequencies characteristics of the HVSR curves. More specifically, these criteria concern the window length, the multitude of the temporal windows, the number of significant cycles, the standard deviation of the peak amplitude, the sharpness of the peak together with its corresponding frequency, and the amplitude of the standard deviation. When these criteria were fulfilled, the frequency of the peak was adopted as the fundamental frequency response of the site. The corresponding amplification factors were considered hereby but only as indicative proxies of the site's amplification. The main reasons for ~17% of measurements not fulfilling these criteria were transients, two or more peaks of the curve and/or a small amplitude of the peak ($A < 2$; [44]). In cases of small amplitudes and questionable peaks, the decision for adopting them was based upon their consistency with adjacent measurements. A few HVSR curves without any, or having questionable peaks were rejected; it is worth noting that such curves may not result from recording artifacts, but may relate with the geometry of the subsurface geology or the topography (2D or 3D effects). However, the study of such effects is beyond the scope of this work, since it requires a plethora of geotechnical information which is not available.

Finally, 68 out of 82 points were employed for assessing the site response (Table 1; Fig. 5). Their peak frequencies are distributed in the range 0.7–17 Hz in the study area. Several curves with two clear peaks are observed throughout Paliki Peninsula. These are explained by two velocity impedances, a shallow one, related with high frequency peaks, and a deeper one, located possibly on the bedrock and related with low frequency peaks. As can be observed in Fig. 6, two groups of peaks are found in the investigated area, the first group being in the low frequency band ranging 0.7–4 Hz and the second group in the medium to high frequency band ranging 5.5–17 Hz. Interestingly, a gap exists





between the two amplification frequency bands in the range 4–5.5 Hz, implying for two types of soils with different elastic properties.

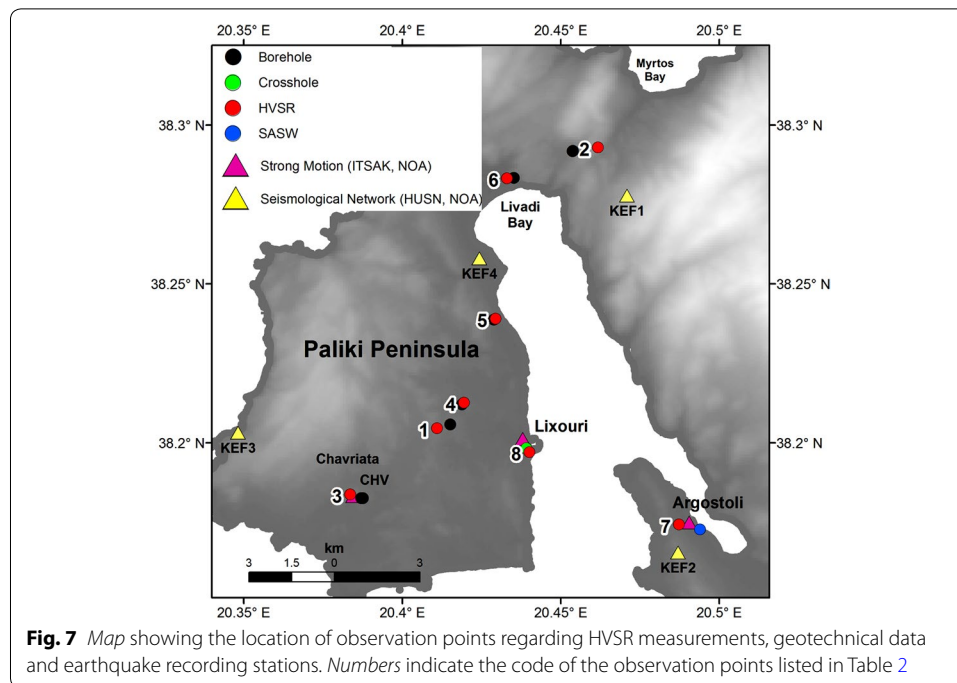
Analysis of geotechnical data

The issue of reliability of the HVSR measurements was examined by comparing them with adjacent boreholes and field measurements of seismic velocities. The information utilized at each borehole was NSPT (Number of Standard Penetration Tests) values observed at various depths. These values were converted into shear-wave velocity (V_s) through an empirical formula proposed by (Tsiambaos and Sabatakakis [48]) which was averaged to obtain simplified 1D models. Seismic velocities in Argostoli were obtained by crosshole surveying [41] and in Lixouri by Spectral Analysis of Surface Waves (SASW) [39]. Table 2 summarizes the geotechnical and geophysical observations used in the current analysis, showing that V_s observations in the epicentral area are compatible

Table 2 Average subsoil characteristics deduced from geotechnical boreholes [51] and field measurements [39, 41]

| 1 | 2 | 3 | 4 | 5 | 6 | 7 | 8 | 9 |
|------|------------------|----------------|---------------|---------------|------------------------|------------------------|------------------------|--------------------------|
| Code | Observation type | Soil type | V_s (m/sec) | Thickness (m) | Best fit V_s (m/sec) | Best fit thickness (m) | Theoretical F_0 (Hz) | Observed HVSR F_0 (Hz) |
| 1 | Borehole | Clay with sand | 247 | 5.5 | 250 | 6 | 12 | 13 |
| 2 | | Clay rumble | 285 | 7 | 282 | 26 | 2.4 | 2.1 |
| 3 | | Marl | 363 | 13 | 379 | 16.5 | 2.1 | 2 |
| 4 | | Clay-marl | 320 | 4 | 305 | 12 | 6 | 5 |
| 5 | | Clay-marl | 329 | 15 | 343 | 42 | 2 | 2.1 |
| 6 | | Clay rumble | 294 | 7.5 | 300 | 10 | 7 | 6.5 |
| 7 | Crosshole | Clay | 280 | 10 | 242 | 18 | 2 | 2 |
| 8 | SASW | Clay | 260 | 8 | 235 | 12 | 4 | 3.3 |

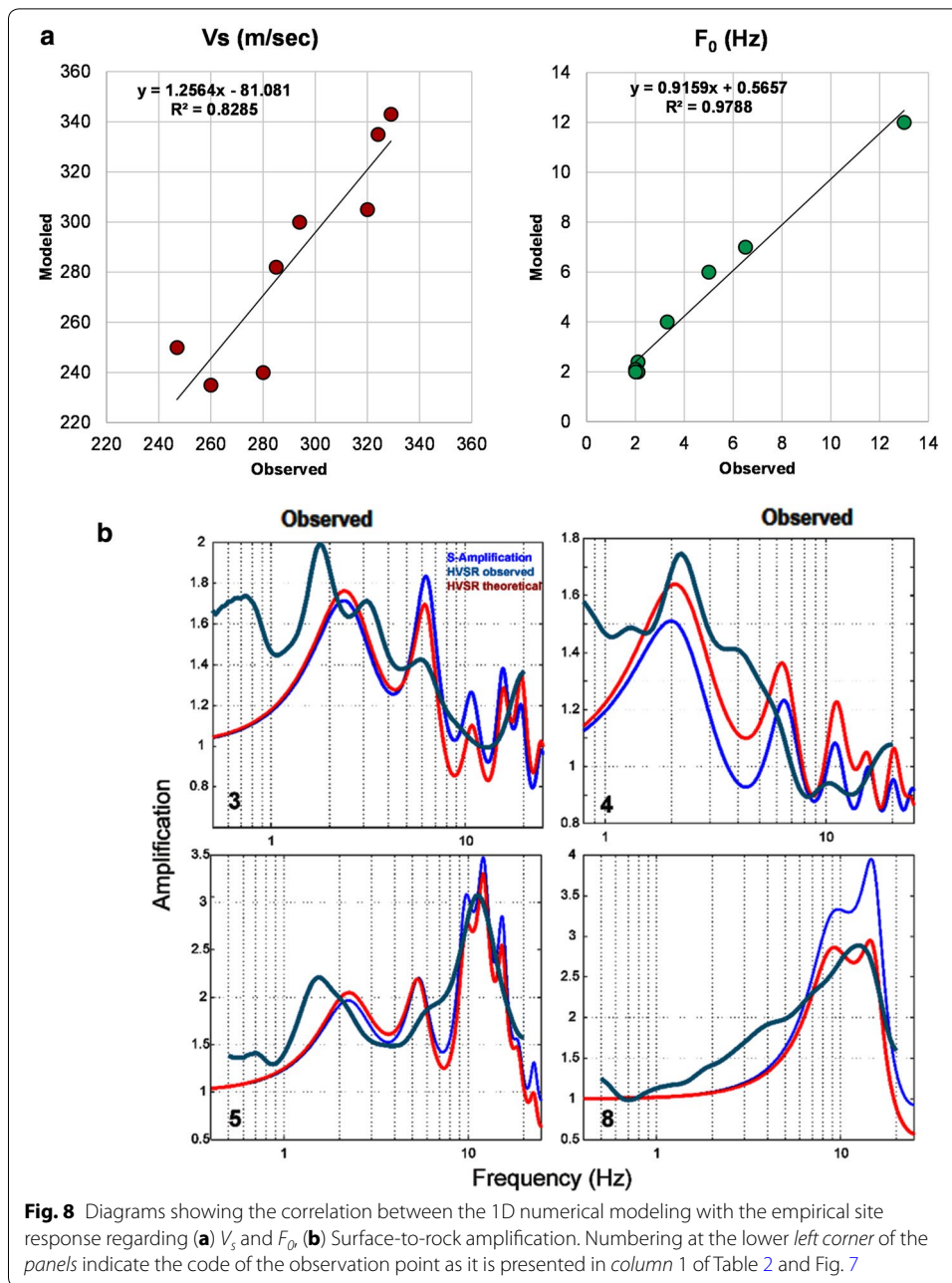
Column 1 refers to the code of the observation points shown in Fig. 7. Column 5 refers to the penetration depth of the boreholes and the bedrock-surface distance for SASW and crosshole models. F_0 denotes the soil column peak frequency



with soils of class B according to [9] and Eurocode 8 (EC8; CEN/TC250/SC8/N317, 2001) [10].

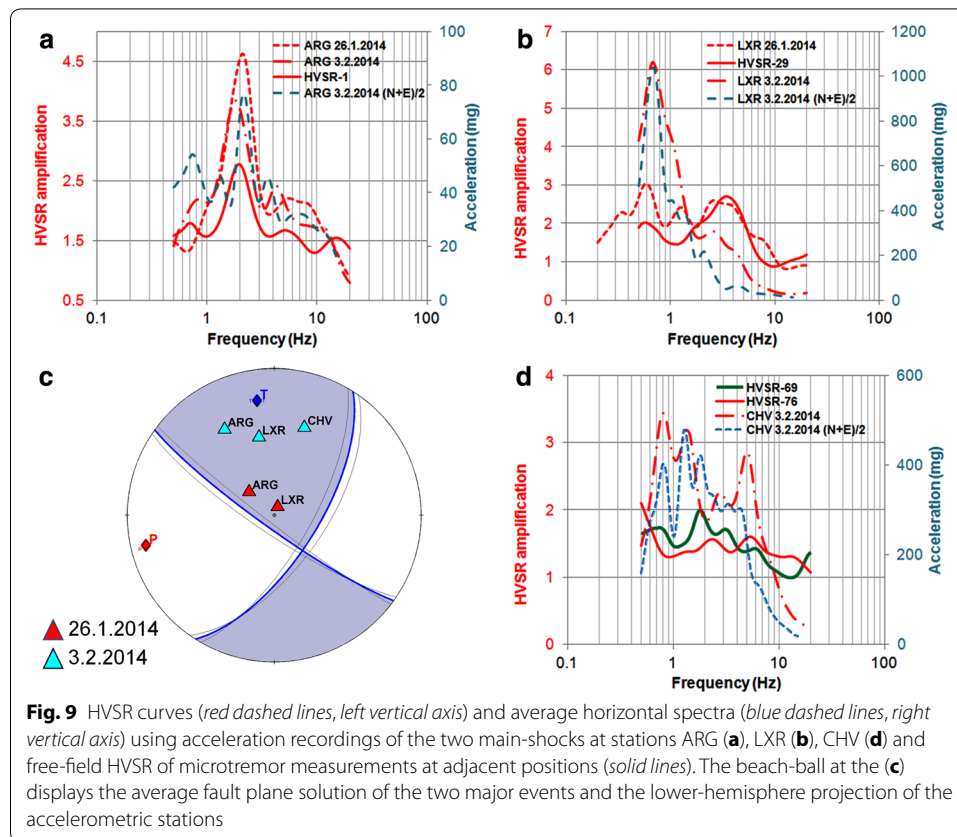
Theoretical 1D soil response (horizontal, vertical and their ratio) was calculated using the ModelHVSR software, a suite of MatLab routines for the analysis and interpretation of ambient noise measurements [19]. A one-layer visco-elastic model overlying half-space was considered at each observation point (Fig. 7). The upper layer was parameterized by the inferred V_s and penetration depth of the boreholes and the thickness of the soil column of the crosshole and SASW models (columns 4 and 5 in Table 2). Given the lack of coherent information, generic V_p/V_s and intrinsic parameters were input. The results of this analysis yielded incoherency between borings and adjacent HVSR measurements for the majority of the observation points, as ambient noise HVSR peak frequencies were found to be systematically lower than the response frequencies of the geotechnical models.

We investigated this issue by performing inversion of HVSR observations towards determining a best-fit visco-elastic model at each observation point. The 1D models (columns 4 and 5 in Table 2) were employed as starting models into a Monte-Carlo scheme using ModelHVSR. The procedure was parameterized by allowing a free search of the thickness of the upper layer and a search within 50% of the input V_s value. The results of the 1D linear numerical modeling is close to the empirical site response regarding the shear-wave velocities, V_s , and the peak frequencies, F_0 (columns 6–9 in Table 2; Fig. 8a). This procedure yielded consistent best-fit models (Fig. 8b) which were found to exhibit a larger soil column thickness and hence we suggest that the former discrepancies occurred due to the limited penetration/sampling depth of borings and partly due to the empirical NSPT-to- V_s relation considered.



Analysis of earthquake data

The HVSR technique has been proven an effective and low-cost tool to capture site amplification when applied to both ambient noise and weak earthquake recordings [25, 32, 33]. In contrast, incompatibility in site response derived by the HVSR technique has been proven to increase with the increase of the level of the ground motion excitation [31]. To evaluate the site response calculated from individual free-field short-term HVSR measurements, we investigated their correlation with the corresponding HVSR derived from earthquake signals, taking advantage of events recorded locally during the 2014 aftershock activity.

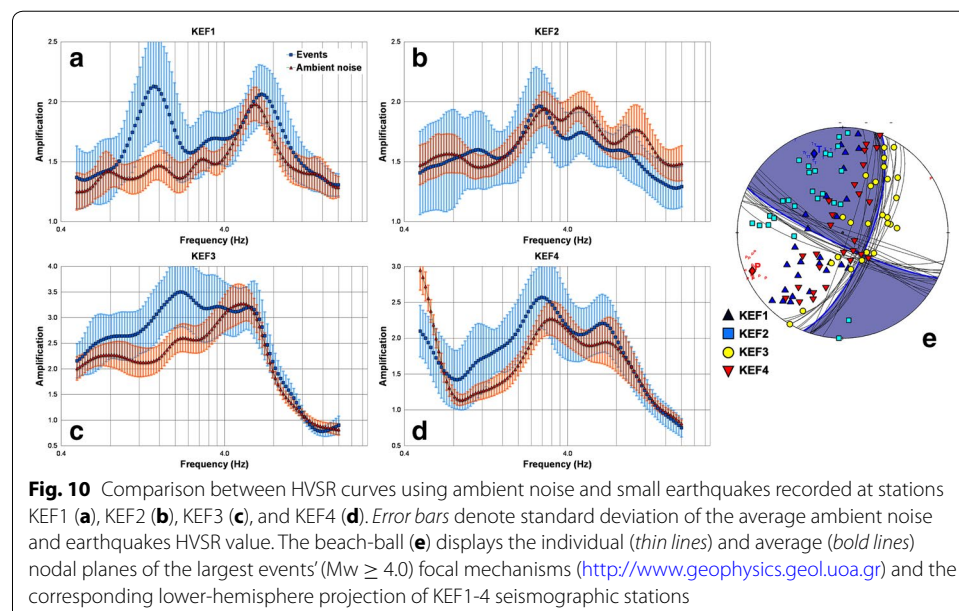


Strong motion HVSR curves were computed at the accelerometric stations ARG (Argostoli), LXR (Lixouri) and CHV (Chavriata), all of them lying on Holocene alluvial deposits (Fig. 2). At station ARG the strong motion (red dashed lines in Fig. 9a) and ambient noise (red solid line in Fig. 9a) HVSR curves exhibit an almost identical peak frequency at about 2 Hz. The amplification ratios of the earthquakes HVSR curves appear proportional to the epicentral distance of the two earthquakes (Fig. 2), with an amplification value of 4.6 for the event on 26.1.2014 (at ~5 km) and a value of 3.7 for the event on 3.2.2014 (at ~11 km), while the amplification deduced from ambient noise (solid red line in Fig. 9a) is found to be lower by about a factor of 2. The peak frequency values are in good agreement with the theoretical linear elastic transfer function based on the V_s profile available from crosshole measurements 0.4 km away from ARG [14, 41]. These findings suggest that it is reasonable to presume a linear site response in Argostoli.

The recordings of the 3.2.2014 event at LXR (red dash-dotted line in Fig. 9b) exhibit high amplification of the ground motion in the low frequency band (0.7 Hz) at a value ~6 and de-amplification at higher frequencies with respect to microtremor measurements at an adjacent site. This pattern is typically correlated with the properties of the seismic source and azimuthal propagation effects, unlikely or maybe partly related to the subsurface geometry and the surface morphology (e.g. [11]). Regarding the event on 26.1.2014 (red dashed line in Fig. 9b) the source-propagation effects at lower frequencies appear limited and good agreement with ambient noise is observed at higher frequencies (~3.5 Hz).

Inconsistency is also indicated at CHV station. Strong motion HVSR for the major event of 3.2.2014 (red dashed line in Fig. 9d) exhibits amplification at a value ~ 4 in the low frequency band, having two peaks at 0.8 and 1.5 Hz. Higher frequencies are not de-amplified, but, on the contrary, a third peak is observed at 5 Hz. No immediate resemblance with the complicated shape of the ambient noise HVSR curves (solid lines in Fig. 9d) is inferred. It is worth mentioning that clear ambient noise HVSR peaks occur when a significant velocity contrast exists at some depth. No well-ordered peaks are likely related to local subsurface structures, which may not exhibit any sharp velocity contrast at any depth, leading to low amplification and/or de-amplification [3, 22]. Irregular surface and subsurface topography have been proposed to exist at CHV to explain the extremely large values of ground acceleration recordings [14]. Taking this into account, although the shapes and amplitudes are significantly different, there is some partial correlation between the frequencies where the main peaks are observed in the accelerometric record of the 3.2.2014 event at CHV and the microtremors HVSR curves. This indicates that the high energy content provided by the major event has excited frequencies that were likely to be relatively more amplified than others at this site, as implied by the amplification curves of the less energetic microtremors.

Aftershock weak-motion recordings were available by a local network comprising 4 broadband stations (KEF1-4), installed in the epicentral area a few days after the first main-shock on 26.1.2014 (Figs. 2, 7). Two stations (KEF2, KEF4) are on soft sediments, one on bedrock (KEF3) and one (KEF1) above the interface between the bedrock and soft sediments. A large number of aftershocks were recorded by this network, covering a wide range of magnitudes and epicentral distances. Herein, we process data during January–September 2014 regarding: (a) waveforms of 80 aftershocks with $M \geq 3$ at different epicentral areas presenting a high quality signal and (b) a large number of ambient noise seismograms for different periods of the year and different hours of the day, in order to include effects from potential sources of transients that might affect the stability of the



results and to ensure their reduction by averaging the large dataset used. Ambient noise and earthquakes HVSR curves were computed using the GEOPSY software.

Figure 10 presents the results of this analysis at each station and some remarkable patterns are exhibited. In general for KEF2 and KEF4 there is good agreement between the HVSR derived from stationary ambient noise and the one from small local earthquakes, with their differences being statistically important (at a 95% confidence interval) for the 35 and 40% of frequency values, respectively. KEF2 and KEF4 are located on a smooth and low topographic relief. On the contrary, at KEF1 and KEF3, which are respectively situated on a steep hill and near a steep cliff, discrepancy occurs at lower frequencies, since earthquake HVSR curves exhibit peaks in the low frequency band (1.7 and 2.1 Hz, respectively), which are not clearly observed at the respective ambient noise HVSR. This is partly explained by topographic effects that can significantly amplify ground excitations at certain frequencies and distances from the relief edge (e.g. [8]). The ambient noise is generally found to cause slight underestimation of the amplification of the sites at most frequencies, but this undervalue is usually near the 1σ bound; thus, we consider both approaches of ambient noise and weak earthquakes HVSR comparable. However, as in the case of accelerometric records, even where the amplification difference is notable, there appears to be some partial correlation in implied peak frequencies between the event and the ambient noise curves. In this regard, the strong peak of KEF1 at ~ 1.5 Hz, despite its significant difference in amplification, matches the frequency of a small peak of the ambient noise curve. Had this peak been less energetic, a smaller one might also be observed at ~ 0.7 – 0.8 Hz, but this has apparently been masked, as indicated by a small increase in the error of the events curve. The same could be said for the main peak of the events curve at KEF3. In this case, a slight increase of the ambient noise curve around 2 Hz indicates a possible peak frequency, which is masked by the much stronger peak at ~ 5 Hz. There is also a good partial correlation in the two shapes in the bands of 1.5–2.1 Hz and in the frequencies lower than ~ 0.75 Hz, while for those higher than 4 Hz there is a match in the amplification despite small differences in shapes.

In an attempt to investigate possible reasons that cause the observed discrepancies, we plot the projection of the focal sphere for the two major events (Fig. 9c) and their largest aftershocks (Fig. 10e). Accelerometric stations lie in the same compressional quadrant (Fig. 9c). For the event on 26.1.2014, ARG and LXR (red triangles in Fig. 9c) are nodal, which would indicate stronger S-wave, but also lie near the null axis of the moment tensor, which reduces the expected S-wave amplitudes according to the radiation pattern. LXR being closer to the null axis than ARG could explain the stronger amplification values observed at ARG for the first major earthquake.

For the event on 3.2.2014, ARG, LXR and CHV (cyan triangles in Fig. 9c) lie near the T-axis of the moment tensor. The expected S-wave H/V ratio, according to the radiation pattern, is smaller at stations ARG and LXR for this event than for the first major earthquake. Indeed, the amplification at station ARG is smaller for the second event, but the opposite is true at station LXR. This indicates that the observed high energy at the lower frequency range around 0.7 Hz at LXR is likely attributed to near-field effects caused by the finiteness of the seismic source, as it is also inferred by the similar distribution of the average horizontal acceleration (blue dashed lines, right axis in Fig. 9) and the strong motion HVSR (solid lines in Fig. 9). Near-field effects at LXR for the event on 3.2.2014

could also be intensified due to its shallower depth (~5 km), despite its slightly smaller magnitude with respect to the deeper event on 26.1.2014 (~16 km depth).

Similar outcome is inferred for the weak motion recordings at stations KEF1-4 by the projection on the focal sphere of several $M_w \geq 4.0$ earthquakes distributed along the activated aftershock zone (Fig. 10e). Stations KEF3 and KEF4 are nearly collinear with the inferred fault trace and they have similar earthquake HVSR curves (panels c and d in Fig. 10). Stations KEF1 and KEF2 are located away from the nodal planes, with the latter being mainly distributed within the T-axis quadrant.

By joint comparison of strong and weak motion data, we conclude that ground motion amplification is likely due to a combination of the source radiation field and site effects. More specifically, it is suggested that: (a) at all earthquake recording sites, lower frequencies (0.7–2 Hz) are amplified, to a larger (KEF1) or lesser extent (KEF3), due to the earthquake source and seismic wave propagation effects, whilst for higher frequencies (>4 Hz), site effects are presumably responsible for the high amplification; (b) at sites ARG, KEF2, KEF4 local conditions likely amplify the low frequency band (0.7–2 Hz) as well.

Discussion and conclusions

We investigate site effects in Cephalonia Island, which is the most seismically prone area in the SE Mediterranean, having suffered several devastating earthquakes, the greatest of which with magnitudes of the order of M7. Two moderate magnitude earthquakes in early 2014 generated extended structural damage and environmental effects, as well as the highest ground acceleration values ever recorded in Greece motivated our effort towards examining the effects of local conditions in the seismic wavefield. For this scope, we analyzed: (a) free-field ambient noise measurements obtained through an in situ survey performed in May 2014, (b) data from geotechnical boreholes located along the main roads in the study area [51], (c) geophysical profiles [39, 41], (d) acceleration recordings of the two main events and (e) aftershocks weak motion recordings from four stations located in the epicentral area. Below, we summarize the followed procedure and the most important findings of this work.

Free-field three-component ambient noise records at 82 positions in the meizoseismal area were analyzed using the HVSR method [32]. Most of the resulted HVSR diagrams exhibit clear peaks, suggesting significant velocity impedance between the upper layers and the bedrock. A few flat HVSR curves are observed, implying for no site amplification. Clear resonant peaks are in the frequency range 0.7–17 Hz, which is within the range of the natural frequencies of most of the buildings. Quasi-amplification factors are found to range between 1 and 7. Resonant peaks are distributed within two frequency zones, a low (0.7–4.0 Hz) and medium–high one (5.5–17 Hz). These observations clearly imply for two types of soils with different elastic properties. In general, low-frequency peaks correlate with Quaternary deposits and high-frequency ones correlate with carbonate bedrock; however, a clear association cannot be established. Several HVSR curves with two clearly separated peaks are observed throughout Paliki Peninsula and they are attributed to distinct shallow and deep velocity impedance contrasts [16]. Curves with irregular peaks are suggested to relate with a smooth velocity gradient of the subsurface structures leading to low amplification [3, 22].

The reliability of the empirical site response range was examined by elastic 1D linear numerical modeling using V_s deduced from geophysical surveying and geotechnical boreholes. The theoretical soil response of both the boreholes and the geophysical models is found to be consistent with the empirical HVSR response. Some incompatible cases regarding boreholes are explained by (a) restrictions of the NSPT technique, (b) extremely localized 1D conditions, and (c) the small depth of drilling, not providing sufficient information about the surface to bedrock distance.

The stability of our measurements was investigated by comparing them with HVSR computed from local recordings of the 2014 main-shocks at stations ARG, LXR, CHV and their aftershocks at stations KEF1-4. At station ARG, located above alluvial deposits in Argostoli, strong motion and ambient noise HVSR curves exhibit an almost identical peak frequency at about 2 Hz. These are also consistent with the theoretical elastic transfer function available from crosshole measurements conducted nearby [14, 41]. The discrepancy between earthquake motion and ambient noise amplification is attributed to nonlinear soil response. Hence, we suggest that site conditions in Argostoli likely amplifies strong ground motion at ~ 2 Hz.

At station LXR, located above soft soil deposits in Lixouri, the observed pattern is inconsistent, especially for the second main-shock on 3.2.2014. The most complex configuration is indicated at CHV station, where apparently no correlation with ambient noise HVSR is found. The HVSR peaks arrangement at both stations is likely related with the spectral content of the maximum recorded horizontal acceleration reaching ~ 0.8 g at CHV, a value that has been attributed to near-field effects by Theodoulidis et al. [46]. However, at a closer look, some of the peak frequencies excited by the major event on 3.2.2014 are consistent with existent peaks in the HVSR curve, although they might be weak.

The analysis of 80 aftershocks time histories of the 2014 series with magnitudes $M \geq 3$, and numerous noise signals recorded at stations KEF1-4, located in the epicentral area, revealed many similarities between the HVSR curves of the two datasets. A good agreement is manifested for both the resonant frequencies and amplification at stations KEF2 and KEF4, located on soft soil. Inconsistency, attributed to the source radiation pattern, was mainly observed at low frequencies at the seismological stations KEF1 and KEF3 for local small earthquakes as well as at the accelerometric stations LXR and CHV for the major events, possibly due to near-field effects. The amplification of the ambient noise and the earthquakes HVSR curves is of comparable magnitude at higher frequencies, with the latter being slightly higher, although lying within the uncertainty range of measurements. The best match between HVSR curves of noise and local small events are found for KEF2, situated in Argostoli, confirming the matching observations at ARG. For clarity reasons, the aforementioned are summarized in Tables 3 and 4.

Despite the near-source effects, the observed particularity of strong ground motion frequency and amplification characteristics may be likely explained by a soil nonlinear behavior for frequencies lower than 2 Hz. Hartzell et al. [17], by performing numerical analysis regarding the interaction between various ground excitations and 1D soil models, came to the conclusion that a nonlinear formulation is needed for site classes D and E and for site classes BC and C, found in the study area, with input motions greater than a few tenths of the acceleration of gravity.

Table 3 Interpretation of the HVSR of strong ground motion with respect to the theoretical seismic energy radiation pattern deduced from moment tensors of the 2014 Cephalonia earthquake sequence (see Fig. 9)

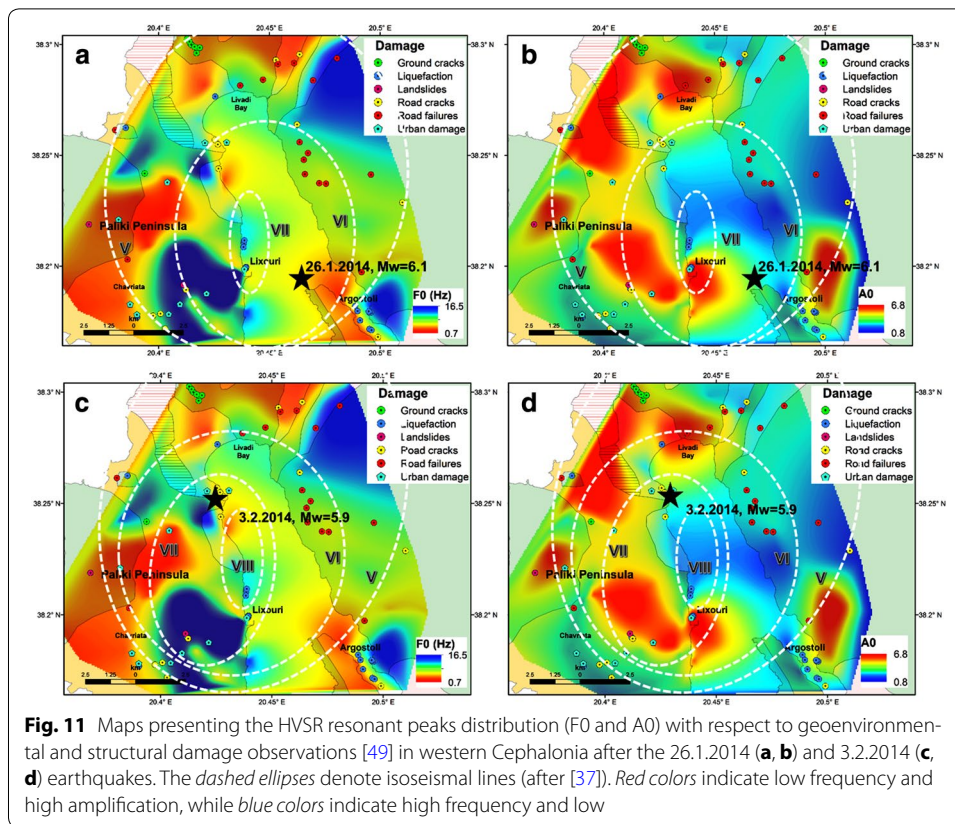
| Station | Peak freq. (Hz) | Cause |
|--------------|-----------------|-----------------|
| EQ 26/1/2014 | | |
| ARG | 2 | Source and site |
| LXR | 3.5 | Source and site |
| | 0.6 (minor) | Source and site |
| EQ 3/2/2014 | | |
| ARG | 2 | Source and site |
| LXR | 0.7 | Source and site |
| CHV | 0.8 | Source and site |
| | 1.5 | Source and site |
| | 5 | Site |
| | 1.9 (N + E) | Source and site |

Table 4 Summary and interpretation of the comparison between weak earthquake and ambient noise data with respect to the theoretical seismic energy radiation pattern deduced from moment tensors of the 2014 Cephalonia earthquake sequence (see Fig. 10)

| Station | Comments | Radiation pattern | Amplitude difference (%) | Correlation coefficient (>0.8) (%) | Peak freq. (Hz) | Cause |
|---------|---------------------------------------|--------------------------------------|--------------------------|------------------------------------|-----------------|-----------------|
| KEF1 | Match at f < 0.9 Hz or f > 5 Hz | Farthest from fault plane | 31 | 64 | 1.7 | Source and site |
| | | | | | 6.5 | Site |
| KEF2 | Best matching | Compressive quadrant | 35 | 46 | 2.8 | Source and site |
| KEF3 | Source effect at f < 4 Hz | Fault plane | 60 | 47 | 2.1 | Source and site |
| KEF4 | Best matching at f > 4 Hz | Mid. distance from fault plane | 43 | 70 | 2.8 | Source and site |

Dimitriu et al. [7] applied the HVSR method to (mostly near-field) acceleration data recorded at a soil site in the town of Lefkas (western Greece) and found an impressive increase in the site's effective resonance period with increasing excitation level. They divided this effect of nonlinearity into three distinct frequency bands; (a) till about 1.3 ± 1.8 Hz, where the strong-motion (nonlinear) response exceeds the weak-motion (linear) one (b) between ~ 2 and 4 Hz, where the nonlinear response falls below the linear one and (c) above ~ 4 Hz where the nonlinear response drops under unity (de-amplification). For frequencies above ~ 10 Hz, the two responses were found to converge. Such a configuration may likely explain the discrepancies between weak earthquake and ambient noise excitations which were observed in the present study.

Figure 11 summarizes the site response in western Cephalonia derived by the combination of 68 HVSR curves using a nearest neighbor module within an Arc-GIS mapping scheme. Superimposed macroseismic observations during the 2014 main-shocks are after Papadopoulos et al. [37] and Valkaniotis et al. [49]. A smooth lateral distribution of peak values is observed with a general trend of low frequency peaks to be correlated with soft sediments and high frequency peaks with hard carbonate rocks. No



clear correlation with surface geology is inferred for the southern Paliki Peninsula where high resonant frequencies (>5 Hz) and low amplification are observed. A general trend inferred in Fig. 11 is that coseismic effects [49] are related with high frequency peaks and low amplification. We suggest that the acquired pattern in these areas can be explained by the existence of thin sediments combined with effects related to the complex geometry of the topographic relief. In this context, the areas of Livadi and southeast Paliki are likely susceptible to nonlinear amplification triggered by near earthquakes. Structural damage can likely be explained by soil-structure interaction, as the fundamental frequency of the soil matched that of the typical eigenfrequencies of one-, two- and three-story buildings that were mainly damaged in the epicentral area, lying in the range between 3 and 10 Hz.

A delineation of low HVSR frequency peaks in a rough NNE-SSW direction, consistent with the strike of the activated fault as it was defined by Karakostas et al. [20] among others, implies for thin and loose soil formations. The pattern is consistent with Cochran et al. [5] who indicate that faults can affect rock properties at substantial distances from slip surfaces and throughout much of the seismogenic zone by reducing the shear moduli and seismic velocities of the rocks. Such an arrangement involving a weakened uppermost crust might better explain the observed vertical GPS deformation distribution, suggested to be attributed to a small “normal-fault” component along the upper part of the fault planes [42].

The resulted ambient noise HVSR are considered to be capable of representing the soil response at the measured sites in the study area, and hence could be alternative and/or complementary to geotechnical models towards constructing realistic shake-map scenarios and risk models in western Cephalonia, taking advantage of the high resolution image of the seismogenic zone deduced from the recent activity. Inconsistencies observed in the low-frequency range at some sites, likely due to near-field earthquake excitations, or effects related to the source radiation pattern should be taken into consideration.

Acknowledgements

This work was funded by EPPO-ITSAK. We are thankful to E. Dimou, member of the Geotechnical Division of the Ministry of Environment, Energy and Climate Change (YPEKA) for providing the borehole data used herein. We thank V. Mitropoulou and A. Lagopati for their help in the field survey and collection of data. We are grateful to Dr. N. Malakatas, director of the Central Research Institute of YPEKA and I. Vasileiou for helping us with their manipulation. We thank EPPO-ITSAK and NOA-GI for providing strong motion recordings and waveform data from a local network, respectively. We appreciate comments from A. Ganas. We thank I. Misailidis and G. Sakkas for providing the GIS digital geotechnical map.

Authors contributions

IK carried out field work, data analyses, and writing the manuscript; PP carried out field work, data analyses and review of the manuscript; VK carried out data analyses and co-writing the manuscript; NV carried out data analyses and review of the manuscript. All authors read and approved the final manuscript.

Competing interests

The authors declare that they have no competing interests.

Publisher's Note

Springer Nature remains neutral with regard to jurisdictional claims in published maps and institutional affiliations.

Received: 16 October 2016 Accepted: 3 April 2017

Published online: 14 April 2017

References

1. Apostolidis P (2002) Determination of the sub-soil structure using microtremors. Application to the estimation of dynamic properties and geometry of the soil formations at Thessaloniki city. Ph.D., Aristotle University of Thessaloniki. **(in Greek with an English abstract)**
2. Bard P-Y (1999) Microtremor measurements: a tool for site effect estimation? In: Irikura K, Kudo K, Okada H, Sasatani T (eds) The effects of surface geology on seismic motion. Balkema, Rotterdam, pp 1251–1279
3. Bonnefoy-Claudet S, Cornou C, Bard P-Y, Cotton F, Moczo P, Kristek J, Fah D (2006) H/V ratio: a tool for site effects evaluation. Results from 1-D noise simulations. *Geophys J Int* 167:827–837
4. Bornovas I, Rontogianni-Tsiabaou T (1983) Geological map of Greece. Institute of Geology and Mineral exploration, Athens
5. Cochran ES, Li Y-G, Shearer PM, Barbot S, Fialko Y, Vidale JE (2009) Seismic and geodetic evidence for extensive, long-lived, fault damage zones. *Geology* 37(4):315–318
6. Diagourtas D, Tzanis A, Makropoulos K (2001) Comparative study of microtremors analysis methods. *Pure Appl Geophys* 158:2463–2479
7. Dimitriu P, Kalogeras I, Theodulidis N (1999) Evidence of nonlinear site response in horizontal-to-vertical spectral ratio from near-field earthquakes. *Soil Dyn Earthq Eng* 18:423–435. doi:10.1016/S0267-7261(99)00014-7
8. Douglas J, Seyedi DM, Ulrich T, Modaresi H, Foerster E, Pitilakis K, Pitilakis D, Karatzetzou A, Gazetas G, Garini E, Loli M (2015) Evaluation of seismic hazard for the assessment of historical elements at risk: description of input and selection of intensity measures. *Bull Earthq Eng* 2015(13):49–65
9. EAK (2003) Greek seismic code. In: Earthquake planning and protection organization. Athens, 7 appendixes, p 72 **(in Greek)**
10. Eurocode 8 (CEN) (2001) prEN 1998-1—Eurocode 8: design of structures for earthquake resistance. Part 1: General rules, seismic actions and rules for buildings. DRAFT No 3, Doc CEN/TC250/SC8/N288, May 2001, Brussels
11. Field EH, Kramer S, Elgamal AW, Bray JD, Matasovic N, Johnson PA, Cramer C, Roblee C, Wald DJ, Bonilla LF, Dimitriu PP, Anderson JG (1998) Nonlinear site response: where we're. *Seismol Res Lett* 69:230–234
12. Ganas A, Oikonomou A, Tsimi C (2013) NOAFAULTS: a digital database for active faults in Greece. In: Bulletin of the geological society of Greece, vol. XLVII and Proceedings of the 13th International Congress, Chania, September 2013
13. Ganas A, Cannavo F, Chousianitis K, Kassaras I, Drakatos G (2015) Displacements recorded on continuous GPS stations following the 2014 M6 cephalonia (Greece) earthquakes: dynamic characteristics and kinematic implications. *Acta Geodyn Geomater* 12(1):177

14. GEER/EERI/ATC (2014) Earthquake Reconnaissance January 26th/February 3rd 2014 Cephalonia, Greece Events, Version 1: June 6, 2014
15. Gosar A (2008) Site effects study in shallow glaciofluvial basin using H/V spectral ratios from ambient noise and earthquake data; the case of Bovec basin (NW Slovenia). *J Earth Eng* 12:17–35
16. Gosar A (2010) Site effects and soil-structure resonance study in the Kobarid basin (NW Slovenia) using microtremors. *Nat Hazards Earth Syst Sci* 10:761–772
17. Hartzell S, Bonilla LF, Williams RA (2004) Prediction of nonlinear soil effects. *Bull Seismol Soc Am* 94(5):1609–1629
18. Hatzfeld D, Kassaras I, Panagiotopoulos D, Amorese D, Makropoulos K, Karakaisis G, Coutant O (1995) Microseismicity and strain pattern in NW Greece. *Tectonics* 14:773–785
19. Herak M (2008) ModelHVSRA—A Matlab® tool to model horizontal-to-vertical spectral ratio of ambient noise. *Comput Geosci* 34:1514–1526
20. Karakostas V, Papadimitriou E, Mesimeri M, Gkaraouni C, Paradisopoulou P (2014) The 2014 Kefalonia doublet (Mw6.1 and Mw6.0), Central Ionian Islands, Greece: seismotectonic implications along the Kefalonia transform fault zone. *Acta Geophys*. doi:10.2478/s11600-014-0227-4
21. Kassaras I, Kalantoni D, Kouskouna V, Pomonis A, Michalaki K, Stoumpos P, Mourloukos S, Birmpilopoulos S, Makropoulos K (2014) Correlation between damage distribution and soil characteristics deduced from ambient vibrations in the old town of Lefkada (W. Greece). In: Second European conference on earthquake engineering and seismology (2ECEEES), Istanbul, Paper No 251
22. Konno K, Ohmachi T (1998) Ground-motion characteristics estimated from spectral ratio between horizontal and vertical components of microtremor. *Bull Seismol Soc Am* 88(1):228–241
23. Koukis G, Andronopoulos V, Rozos D, Kinigalaki M, Tzitziras A, Pogiati E, Garivaldi A (1993) Engineering map of Greece, in 1:500,000 scale, IGME, Athens
24. Lachet C, Hatzfeld D, Bard P-Y, Theodoulidis N, Papaioannou C, Savvaidis A (1996) Site effects and microzonation in the city of Thessaloniki (Greece): comparison of different approaches. *Bull Seismol Soc Am* 86(6):1692–1703
25. Lermo J, Chávez-García FJ (1993) Site effect evaluation using spectral ratios with only one station. *Bull Seismol Soc Am* 83:1574–1594
26. Leventakis GA (2003) Microzonation study of the city of Thessaloniki. PhD, Aristotle University of Thessaloniki, **(in Greek with an English abstract)**
27. Makropoulos K, Kassaras I, Stournaras G, Kapourani E, Valadakis E, Plessas S (2004) Results from a multidisciplinary microzonation study in the city of Mytilene (Lesvos Island, Greece). In: Proceedings of the 10th international congress of the geological society of Greece, Thessaloniki, pp 484–485, 15–17 April 2004
28. Makropoulos K, Kaviris G, Kouskouna V (2012) An updated and extended earthquake catalogue for Greece and adjacent areas since 1900. *Nat Hazards Earth Syst Sci* 12:1425–1430
29. Mucciarelli M (1998) Reliability and applicability of Nakamura's technique using microtremors: an experimental approach. *J Earthq Eng* 2(04):625–638
30. Mucciarelli M, Gallipoli MR (2001) A critical review of 10 years of microtremor HVSR technique. *Boll Geof Teor Appl* 42(3–4):255–266
31. Mucciarelli M, Gallipoli MR (2004) The HVSR technique from microtremor to strong motion: empirical and statistical considerations. In: 13th World Conference on earthquake engineering Vancouver, B.C., August 1–6, 2004, Paper No. 45
32. Nakamura Y (1989) A method for dynamic characteristics estimation of subsurface using microtremor on the ground surface. *Q R RTRI* 30(1):25–33
33. Nakamura Y (2000) Clear identification of fundamental idea of Nakamura's technique and its applications. In: Proceedings of 12th world conference on earthquake engineering, Auckland
34. Panou A, Theodoulidis N, Hatzidimitriou P, Stylianidis K, Papazachos C (2005) Ambient noise horizontal-to-vertical spectral ratio in site effects estimation and correlation with seismic damage distribution in urban environment: the case of the city of Thessaloniki (Northern Greece). *Soil Dyn Earth Eng* 25:261–274
35. Paolucci E, Albarello D, D'Amico S, Lunedei E, Martelli L, Mucciarelli M (2015) A large scale ambient vibration survey in the area damaged by May–June 2012 seismic sequence in Emilia Romagna, Italy. *Bull Earthq Eng* 13(11):3187–3206
36. Papadimitriou P, Voulgaris N, Kouskouna V, Kassaras I, Kaviris G, Pavlou K, Karakonstantis A, Bozionelos G, Kapetanidis V (2014) The Kefallinia Island earthquake sequence January–February 2014. Abstract, 2nd ECEEES, Istanbul, Turkey
37. Papadopoulos GA, Karastathis VK, Koukouvelas I, Sachpazi M, Baskoutas I, Chouliaras G, Agalos A, Daskalaki E, Minadakis G, Moschou A, Mouzakiotis A, Orfanogiannaki K, Papageorgiou A, Spanos D, Triantafyllou I (2014) The Cephalonia, Ionian Sea (Greece), sequence of strong earthquakes of January–February 2014: a first report. *Res Geophys* 4(1):19–29
38. Papazachos B, Papazachou K (2003) The earthquakes of Greece. Ziti publ, Thessaloniki
39. Pelekis PC (2014) Comparative evaluation of results of surface methods for determination dynamic properties of soil at seismic recording sites. Research in "Archimedes III," Operational Program "Education & Lifelong Learning" co-financed by EU/Greece
40. Rodriguez VHS, Midorikawa S (2002) Applicability of the H/V spectral ratio of microtremors in assessing site effects on seismic motion. *Earthq Eng Struct Dyn* 31:261–279
41. Rovithis E, Ptilakis K (2011) Seismic performance and rehabilitation of old stone bridges in earthquake-prone areas: the case of Debosset Bridge in Greece. In: Proceedings, innovations on bridges and soil-bridge interaction (IBSBI). Athens
42. Sakkas V, Lagios E (2015) Fault modelling of the early-2014 ~ M6 earthquakes in Cephalonia Island (W. Greece) based on GPS measurements. *Tectonophysics*. doi:10.1016/j.tecto.2015.01.010
43. Scherbaum F, Ohrnberger M, Savvaidis A, Panou A, Theodoulidis N (2002) Determination of shallow shear wave velocity profiles using ambient vibrations at selected sites in Greece, Poster at the A.G.U
44. SESAME (2004) Guidelines for the implementation of the H/V spectral ratio technique on ambient vibrations: measurements, processing and interpretation, <http://sesame-fp5.obs.ujfgrenoble>

45. Stucchi M, Rovida A, Gomez Capera AA, Alexandre P et al (2012) The SHARE European earthquake catalog (SHEEC) 1000–1899. *J Seismol*. doi:[10.1007/s10950-012-9335-2](https://doi.org/10.1007/s10950-012-9335-2)
46. Theodoulidis N, Karakostas C, Lekidis V, Makra K, Margaris B, Morfidis K, Papaioannou C, Rovithis E, Salonikios T, Savvaidis A (2015) The Cephalonia Greece January 26 (M6.1) and February 3 2014 (M6.0) earthquakes: near-fault ground motion and effects on soil and structures. *Bull Earth Eng*, 14(1): 1–38. doi: [10.1007/s10518-015-9807-1](https://doi.org/10.1007/s10518-015-9807-1)
47. Triantafyllidis P, Theodoulidis N, Savvaidis A, Dimitriou P (2006) Site effects estimation using earthquake and ambient noise data: the case of Lefkas town. In: Proceedings of the first European conference on earthquake engineering and seismology, Geneva, 3–8 September 2006, paper 1249
48. Tsiambaos G, Sabatakakis N (2011) Empirical estimation of shear wave velocity from in situ tests on soil formations in Greece. *Bull Eng Geol Environ* 70:291–297
49. Valkaniotis S, Ganas A, Papathanassiou G, Papanikolaou M (2014) Field observations of geological effects triggered by the January–February 2014 Cephalonia (Ionian Sea, Greece) earthquakes. *Tectonophysics* 630:150–157
50. Wyss M, Rosset P (2013) Mapping seismic risk: the current crisis. *Nat Hazards* 68:49–52. doi:[10.1007/s11069-012-0256-8](https://doi.org/10.1007/s11069-012-0256-8)
51. YPEKA (2014) Restoration of the road network in Cephalonia Prefecture after the 2014 earthquakes, Contract #7, Technical Report, **(in Greek)**

Submit your manuscript to a SpringerOpen[®] journal and benefit from:

- ▶ Convenient online submission
- ▶ Rigorous peer review
- ▶ Immediate publication on acceptance
- ▶ Open access: articles freely available online
- ▶ High visibility within the field
- ▶ Retaining the copyright to your article

Submit your next manuscript at ▶ [springeropen.com](https://www.springeropen.com)
